Maghsoudi, M.; Ziehmer, M.; Lilleodden, E.:
Detwinning-mediated hardening in Mg: A microcompression study of a single twin boundary.
In: Materials Science and Engineering A. Vol. 772 (2020) 138747.

First published online by Elsevier: 29.11.2019

https://dx.doi.org/10.1016/j.msea.2019.138747

Detwinning-mediated hardening in Mg: A microcompression study of a single twin boundary

Mohammadhadi Maghsoudi[a,*], Markus Ziehmer[a] and Erica T. Lilleodden[a,b]

[a]Helmholtz-Zentrum Geesthacht, Institute of Materials Research, Materials Mechanics, 21502 Geesthacht, Germany
[b]Hamburg University of Technology, Institute of Advanced Ceramics, 21073 Hamburg, Germany

Abstract

We present the first experimental measurement of the hardening arising from the detwinning of a single twin boundary in Mg. Microcompression tests were performed on two sets of microcolumns: (*i*) single crystals having a "parent" grain orientation of nearly (0 0 0 1) along the compression axis, and (*ii*) bicrystals involving the parent grain and a single $\{1\ 0\ \bar{1}\ 2\}$ twin boundary. A comparison of the stress-strain data shows significant differences in the deformation characteristics of the deformed microcolumns. The bicrystalline microcolumns undergo detwinning, as indicated by a stress plateau, which leads to a nominally single crystalline microcolumn of the orientation of the parent grain. Microcompression beyond the plateau shows that the detwinned microcolumns exhibit a considerably higher yield stress and strain hardening rate than the single crystalline "parent" microcolumns. Electron back-scattered electron analyses on the cross-sections of the deformed microcolumns reveal higher misorientations in the detwinned region indicative of a high content of unpaired dislocations (so-called GNDs), compared to the deformed parent microcolumns. This discrepancy in misorientation distribution between the samples is consistent with a detwinning-mediated hardening response, as observed, and points to the creation of dislocation debris as a consequence of the detwinning process.

Keywords: Micromechanics; Magnesium; Twinning; Work hardening

* Corresponding author.
E-mail address: Mohammadhadi.maghsoudi@hzg.de (M.H. Maghsoudi)

Present address: Helmholtz-Zentrum Geesthacht, Institute of Materials Research, Materials Mechanics, 21502 Geesthacht, Germany
Tel: +49 (0)4152 87-2646

1. Introduction

Dating back to the classical reviews on deformation twinning in hexagonal close-packed (HCP) metals reported by Kocks and Westlake from 1967 [1] and later by Yoo and Lee from 1991 [2], deformation twinning in Mg is well recognized as an important deformation mechanism. Due to the strong anisotropy in the critical resolved shear stresses on the various dislocation slip systems, deformation twinning helps to satisfy the Taylor [3] criterion requiring five independent slip systems for an arbitrary shape change [1, 4]. More specifically, twinning modes can accommodate strain along the $\langle c \rangle$ direction, which is not achievable through the slip systems having $\langle a \rangle$ type Burgers vector [5, 6].

It is well established that the boundaries of a $\{1\ 0\ \bar{1}\ 2\}$ tensile twin, the most activated twin type in Mg with a *c/a* ratio less than $\sqrt{3}$ [7, 8], are generally mobile [9]. Hence, twin boundary migration may either lead to thickening or shrinkage of the twin under straining [9]. Detwinning is associated with the disappearance of existing twin bands under reverse loading [8]. Several aspects of detwinning in Mg have already been studied. On the cyclic loading behavior, Cáceres et al [10] showed large stress-strain hysteresis loops under cyclic loading of an AZ91 alloy attributing to the partial reversal of $\{1\ 0\ \bar{1}\ 2\}$ twins. By using neutron diffraction experiments to monitor twinning activity, it has been shown that this reversible movement of $\{1\ 0\ \bar{1}\ 2\}$ twin boundaries contributes in a pseudo-elasticity in Mg-8.5 wt.% Al [11] and AZ31 [12] alloys. The driving force for the observed detwinning in these studies has been discussed in terms of internal stress development resulting from twinning activity. The mobile character of twin boundaries has been regulated through annealing treatments. In this regard, Nie et al.

[13] showed that the deformation twins can be pinned by segregation of solute elements in twin boundaries during annealing and the resultant pinning effect of solutes on twin boundaries would strengthen the alloys. Other researchers have further investigated this pinning effect in terms of the impacts of deformation condition and solute content [9, 14-16].

Wang and Huang [17] examined the tensile behavior of a pre-compressed AZ31 alloy and found a pronounced increase of the hardening rate as a result of the detwinning of previously formed twins. In line with this finding, Sarker and Chen [18] recently pointed out that detwinning is represented by an increased strain hardening rate that could be explained by strong dislocation-twin boundary interactions. On the contrary, as explicitly discussed by the papers of Cáceres et al. [19, 20], profuse twinning has little or no effect on the overall strain hardening behavior of Mg polycrystals. This has been argued to be due to the small value of the Hall-Petch hardening associated with grain segmentation by twin boundaries, along with the weak role that twin boundaries play as a barrier to dislocations in Mg. Common to all of these experiments is that the reported strain hardening associated with detwinning (or twinning) is influenced by the polycrystallinity of the samples; neighboring grains lead to variations in the stress field and deformation constraints. Therefore, a true assessment of mechanical characteristics associated with detwinning alone should be carried out where a single twin boundary can be isolated.

In the present study, microcompression testing was used to explore detwinning in pure Mg with an isolated twin boundary. By testing a single twin boundary in micron-sized samples, we quantified the influence of the twin boundary migration on the stress-strain characteristics; the yield stress and strain hardening rate. The mechanical results were then linked to the corresponding deformation structures by analyzing the misorientation distribution maps, an indirect measurement of dislocation structure. The analysis is therefore decoupled from the

collective response of several grains in a typical polycrystalline aggregate with its associated complex stress state.

2. Experiments and analysis

A polycrystalline pure Mg (99.85wt.% Mg) sample with a very coarse grain size of ~700-800 µm was firstly mechanically ground and polished using standard metallographic procedures. The sample was characterized using electron backscatter diffraction (EBSD) in order to identify a crystal orientation of the parent grain of interest and the twin/parent crystallographic relationship. An appropriate twin boundary was identified by considering the Schmid factor such that no additional twinning was expected in the parent grain. For this reason, we investigated the deformation of a twin inside a parent grain subjected to microcompression along an axis close to the [0 0 0 1] direction. The twin studied here has not been introduced by a pre-loading, but rather is remnant from the mechanical polishing process. The deformed surface layer from the mechanical polishing was removed through submerging the sample surface into a 0.5% Nital solution for few seconds. Microcolumns were fabricated in the selected parent-twin region using annular milling with an accelerating voltage of 30 kV and varying currents. Final milling was carried out using a single pass circular milling step using a beam current of 1 nA. in a FEI Nanolab 200 Dualbeam scanning electron and focused ion beam (FIB) microscope (Fig. 1a). A [001] inverse pole figure (IPF) map of the sample surface shown in Fig. 1b characterizes the twin/parent misorientation relationship to be a characteristic of the common tensile twinning in Mg, associated with a rotation of the *c*-axis in the parent grain of about 86° around the [2 $\bar{1}$ $\bar{1}$ 0] axis [21]. ‘Based on the presented IPF map, the parent grain is compressed along the [1 0 $\bar{1}$ 8] direction. This direction is approximately 8° off the *c*-axis. Such a misalignment would allow the easy activation of $\langle a \rangle$ basal dislocations;

the stress required for basal slip is ~8 MPa. However, the basal dislocations are not able to accommodate the applied strain along *c*-[0001] direction, therefore the plastic strain is expected to be governed by pyramidal $\langle c + a \rangle$ slip [22]. EBSD measurements were also conducted on the cross-sections of the selected twin band prior to compression. A [100] IPF map of the sample cross-section represents an inclination of the twin boundary, as shown in Fig. 1b. While the interface inclination with respect to the loading axis plays an important role in studying the dislocation-interface interactions [23, 24], the focus in the current study is on the impact of the twin boundary migration on the mechanical behavior. A typical bicrystalline microcolumn having a nominal mid-plane diameter of 4 µm machined at the $\{1\ 0\ \bar{1}\ 2\}$ tensile twin boundary is shown in Fig. 1c. The twin boundary is located in the center of the microsample. All the fabricated microcolumns had an aspect ratio of height to mid-plane diameter between 3 to 4. A FIB cross-sectional analysis performed on a sacrificial microcolumn revealed a typical taper angle of ~3-4°.

The microcompression tests were conducted with a Nanoindenter XP (Agilent) equipped with a flat-ended conical indenter with a 10 µm diameter circular punch using a constant displacement rate of 0.012 $\mu m.sec^{-1}$ up to different targeted engineering strains of approximately 2.5, 5 and 10%. A total of 16 bicrystalline and 26 single crystalline reference microcolumns were tested in order to show the reproducibility of the experimental data.

Post-mortem microstructural characterization was performed on cross-sections of the deformed microcolumns using a FIB lift-out technique. EBSD measurements were performed at 15 kV acceleration voltage and 2.2 nA beam current using an EDAX/TSL detector operating in a FEI Nanolab 200 Dualbeam microscope at a working distance of 10 mm. The EDAX OIM Analysis™ 7 software was used to process the EBSD data. Various scans were performed on several samples compressed to varying strains using a 50 nm step size.

Figure 2 presents a simplified schematic showing the alignment of the bulk twin and parent grain in relation to the fabricated micocolumns. As is well known, tensile twinning can be activated under a compressive load parallel to the basal plane. Therefore, it is expected that the twin boundary in the microcolumn in Fig. 2a will migrate in response to the compressive stress. The longitudinal strain accommodated by the twinning-induced shear strain is given by [22, 25, 26]:

$$\varepsilon = f_{twin} m \gamma \tag{1}$$

where f_{twin} is the twin volume fraction, and m is the twinning Schmid factor (0.49) and γ is the twinning shear for tension twinning. γ in Mg is 0.129 according to Yoo [27]. Since the thickness of the twin within the bulk material varies along its length, the twin thickness within each micropillar also varies. This also complicates the quantification of the twin volume needed to assess the contribution to the axial strain. Here we use a simplified model based on the area fraction of the twin to assess the associated strain; based on the alignment of the twin shown schematically in Fig. 2a, the area of the twin that contributes to the axial strain accommodation of the microcolumn is determined by the twin thickness (Fig. 2c). The twin volume fraction, f_{twin}, is calculated by the ratio of the twin thickness to the initial microcolumn height (H_0) as follows:

$$f_{twin} \cong \frac{A_{twin}}{A_{column}} = \frac{D \times Twin\ thickness}{D \times H_0} = \frac{Twin\ thickness}{H_0}\ , \tag{2}$$

where A and D are the area and the microcolumn diameter, respectively.

It is importantly acknowledged, however, that in order to accommodate the axial deformation resultant from detwinning, the rest of the microcolumn must also deform [28]. According to the alignment of the twin (Fig. 2a), it is not possible to consider the deformation of the twin independent from the parent grain. This is schematically shown in Fig. 2b.

Nonetheless, the response of the twin can be evaluated in comparison to the single crystalline parent response; influence of the concomitant deformation in the parent grain is addressed later.

3. Results and discussion

Secondary electron (SE) micrographs of single and bicrystalline microcolumns before and after 10% compression are presented in Fig. 3. Fig. 3a and b show that a massive shearing of material on distinct slip planes is the main morphological characteristic of the compressed microcolumns in the single crystalline parent grain. These slip traces correspond to the basal slip system as is characteristic of the final stages of the *c*-axis microcompression of Mg [22, 29]. The bicrystals, on the other hand, show many small slip steps on the surface of the microcolumn after compression, as is shown in Fig. 3c and d. In this case, the microcolumns have not (yet) experienced such a massive shear instability.

The engineering stress-strain curves obtained from compression of single crystalline (red curves) and bicrystalline (blue curves) microcolumns to a final engineering strain of 10% are presented in Fig. 4. For clarity, only three curves for each condition are shown. The single crystals show highly reproducible stress-strain curves. They deform with a yield point at a stress level close to 180 MPa followed by a jerky-like hardening regime and then a massive strain burst at a stress level of around 365 MPa. The stress-strain curves of the single crystals look like the typical ones found for microcompression of (0 0 0 1) oriented Mg single crystals, already reported by Lilleodden [29] and Byer and Ramesh [30]. In particular, the similarities hold for the trend in hardening. The differences in the stress-strain response might originate from the ~8° offset from the ideal *c*-axis orientation in this work, along with the size of the tested samples and the deformation rates used for microcompression testing. Activation of six equivalent pyramida1 $\pi 2$ slip systems having $\langle c + a \rangle$ Burgers vector is suggested in the

literature to account for the strain hardening observed in compression of (0 0 0 1) single crystals. This is supported by measurements of the resolved shear stress [29], as well as by direct observation of the active slip systems achieved through transmission electron microscopy [22, 30]. The 8° misorientation of the loading axis from the [0 0 0 1] direction is expected to lead to the required shear stress on the basal plane to activate $\langle a \rangle$ basal dislocations; the resolved shear stress on the basal plane at the yield point is around 8 MPa. As suggested by Lilleodden [29], the massive strain burst resultant at the end of deformation is associated with the escape of dislocations on the basal planes, consistent with the SE image in Fig. 3b.

The mechanical response of the bicrystalline microcolumns (blue curves) differs significantly from their single crystalline counterparts (Fig. 4). The stress increases linearly up to a stress plateau ranging from 22 to 70 MPa, followed by a smooth strain hardening up to stress values ranging from 408 to 508 MPa, values significantly higher than those found for the single crystals. The observed stress plateau is similar to that observed by Kim [22], Liu et al. [31], Prasad et al. [32] and Mallmann et al. [25], where the plateaus were found to be associated in part with twin growth. In the case of Kim [22] and Mallmann et al. (5 μm pillars) [25], twinning reorients the crystal into an orientation for easy basal slip, and thus the plateaus also include massive shearing within the twin .

As already shown in Fig. 2a, the volume fraction of the twin in the bicrystals is not the same for all of the microcolumns. For this reason, detwinning in different microcolumns manifests at different plateau stress-strain values. As shown in Fig. 4, both the stress and the strain associated with the plateaus increase with increasing twin thickness. The amount of strain accommodated by detwinning was calculated based on the twin thickness, according to equation (1), using the volume fraction given by equation (2). The results are available in Table 1. In all cases, it is clear that the total plateau strain is larger than the detwinning strain. In other words, the detwinning shear can only be responsible for ~23-35% of the total plateau strain.

The remaining 65-77% axial strain is expectedly due to the accommodation strain of the parent grain, as is schematically described in Fig. 2b.

EBSD measurements were performed on cross-sections of the deformed microcolumns achieved through FIB milling. This was done on several bicrystalline samples compressed to varying strains, as well on several 'parent' single crystal reference microcolumns. The results are presented in Fig. 5. An EBSD map corresponding to the parent grain prior to compression is shown in Fig. 5a. No pre-existing twins are found. The microstructures corresponding to the microcolumns compressed to 2.5 (Fig. 5b), 5 (Fig. 5c) and 10% (Fig. 5d) strain show that deformation of the single crystals is governed by dislocation slip; no evidence of twining is observed. This is consistant with previous *c*-axis microcompression studies of Mg single crystals [22, 29]. An increasing orientation gradient with increasing applied strain is reflected as the color gradient in the IPF maps on the cross-sections of the deformed single crystals. Quantitatively speaking, the angle between the crystal *c*-axis and the loading axis changes from the initial ~8° to ~14° after 10% strain. The deviation of the *c*-axis from the loading direction leads to an increase in the resolved shear stress on the basal planes resulting in the massive basal shear. The configuration of the parent grain and the twin prior to compression is displayed in Fig. 5e. By applying axial compressive load to varying amounts of plastic strain (Figs. 5f-h), it is clearly observed that the initial twin migrates out of the microcolumn. In a 5% compressed microcolumn, the twin has almost disappeared, with only a small trace of twin visible near the surface (Fig. 5g). While a small twin is observed at the base of the pillar (see lower right region of fig. 5g), it is likely that it existed prior to pillar fabrication and would otherwise not contribute significantly to the deformation as the stresses are significantly lower at the base due to pillar taper. As is clearly shown in Fig. 5h, a microcolumn compressed to 10% strain doesn't show any trace of the twin in the cross-section. Consequently, it can be argued that during compression of the bicrystals that the twin re-orients into the nominal parent

orientation and any subsequent straining beyond the plateau region is of a single crystal. It follows that a comparison of the stress-strain behavior of the single crystalline 'parent' microcolumns to those after the plateau regime in the bicrystalline microcolumns gives insight into the impact of detwinning on the strain hardening response of Mg. We limit our interpretation to two characteristic features of the deformation curves beyond the plateau: the (second) yield stress and the work hardening rate.

In the case of microcompression testing, perfect contact between the flat punch and the microcolumn top surface at the onset of deformation is hardly achievable due to surface roughness and small misalignments. This can lead to early plasticity. Such microplasticity is responsible for the typical compliant behavior at the early stages of microcompression testing. For this reason, the usual definition of yield stress using the 0.2% plastic strain offset convention is inappropriate [33]. In this study, we employ the convention suggested by Kupka et al. [34], in which the slope of the load-displacement curve was used as a criterion to define the yield stress. The yield point is defined here as the point where the slope of the loading curve becomes less than a threshold value, taken here to be 45%, of the maximum loading stiffness. We applied this to the 11 single and 6 bicrystalline microcolumns deformed to 10% strain to find out whether the yield stress is affected by detwinning; the results are given in Fig. 6. It should be noted that for the bicrystalline microcolumns the yield point criterion was applied beyond the stress plateau regime, where the orientation of the microcolumn has reversed to the parent orientation through detwinning. For a reliable statistical comparison of the yield stress results, we identified the best distribution function for each set of data. The distribution of the yield stress was plotted in normal, log-normal, Weibull and gamma probability plots. While the limited number of samples in this work, i.e. on average 5 per strain and strain rate, in turn limits how definitive it is [35], the data sets appear to be best described by a normal distribution function. We use it as a basis for comparison of the two sample types. The obtained normal

probability curves in Fig. 6 including ±95% confidence intervals show that the detwinned microcolumns yield at a stress (274.3±70.5 MPa) compared to the single crystalline reference parent microcolumns (181.6±24.7 MPa). The probability plot also reveals that not only do the detwinned microcolumns possess a higher yield stress, they have a larger confidence band relating to a larger standard deviation. The thickness of the pre-existing twins was added to Fig. 6 for the bicrystalline samples in order to show the dependency of the yield stress to twin thickness. It can be seen that the yield stress increases with increasing thickness of the twin. The larger spread in the yield stress data for the bicrystalline microcolumns can be explained by the variation in volume of the detwinned region. To further support the comparison, we consider the cumulative frequency distribution of the yield stress using the Monte-Carlo approach [35], due to the insufficient number of experimental data points for plotting a reliable cumulative frequency curve. Assuming the normal distribution as the best fit to our yield stress data, we randomly generated 1000 normally distributed microcolumn sets. Results of this Monte-Carlo approach are given in Fig. 7. Consistent with the normal distribution approach, the results reveal a significant shift to higher yield stresses for the detwinned bicrystalline microcolumns.

The detwinned Mg crystals not only show a higher yield stress, but they also have higher strain hardening rate than the single crystalline references indicating that detwinning itself impacts strain hardening. Figure 8 shows the variation of the work hardening rate, $= d\sigma/d\varepsilon$, as a function of true stress for two experiments each of single and bicrystalline (after detwinning) microcolumns. Several spikes in θ are found, associated with the strain bursts, which lead to sudden slope changes in the stress-strain response and noise in the data. This is more noticeable for the single crystalline microcolumns, which show large slip steps on the outer surface of the sample, as already shown in Fig. 3. The peak strain hardening rate, θ_{max}, was measured to be 18.9 GPa and 29.5 GPa for the single crystalline and detwinned

microcolumns, respectively. In the case of macro-scale experiments, the strain hardening is found to be nominally 6.0. This holds for polycrystalline samples of Mg alloys [7, 18, 32, 36], as well as bulk single crystalline Mg [37]. While it has been argued that the strain hardening in AM30 was increased due to detwinning [18], the increase is not significant, and it is difficult at best to decouple the response of the detwinning affect from that of the alloying constituents and overall polycrystalline response.

Once detwinning is exhausted, the microcolumn is single crystalline of the same nominal orientation as the parent grain microcolumns. Yet its stress-strain response shows significantly higher flow stress and strain hardening rate. This points to the influence of the detwinning mechanisms on these two charactersitics. While an increase in dislocation content can readily explain an increase in yield stress, this typically leads to a decrease in the strain hardening rate, for the same material, i.e., the strain hardening rate of the parent grain is a concave downward function. Thus, the observations of a simultaneous increase in yield strength and hardening rate cannot be simply explained by the development of dislocation density during the plateau regime. Moreover, while twin boundaries may render a hardening effect in HCP metals, just as grain boundaries do, the loss of the twin boundary negates this type of argument. Something more fundamental to the process of detwinning itself must be considered.

Experimental and modelling studies by Clausen et al. [38] and Proust et al. [39] have shown that once the lattice re-orients to a hard orientation through twinning, as is the case here (Fig. 5), further axial deformation of the re-orientated lattice requires an increase in stress to activate $\langle c + a \rangle$ slip. However, the stress level at the exhaustion of detwinning (~22-70 MPa) is not high enough to activate these non-basal dislocations. In this situation, the microcolumn may experience a linear elastic hardening until the critical resolved shear stress for the pyramidal slip is achieved. It should be mentioned that $\langle a \rangle$ dislocations might be active at the

detwinning exhaustion stress level and therefore, as mentioned earlier, may contribute to plasticity of the microcolumn through the observed plateau. Nevertheless, these basal dislocations do not provide a deformation along the *c*-axis, i.e., the loading axis.

Consideration of the local variations in orientation points to a better explanation. To this end, the common kernel average misorientation (KAM) analysis was applied to the EBSD data to quantify the misorientation distributions. The KAM maps were constructed from the cross-sections shown in Fig. 5 by calculating the average misorientation of every scan point up to its third nearest neighbors. The results are presented in Fig. 9. It is apparent from the maps that the overall misorientation distribution is more heterogeneous in the compressed bicrystalline microcolumns (Figs. 9e-h) compared to the single crystalline references (Figs. 9a-d). At the exhaustion of detwinning, a higher local misorientation is found in the vicinity of the migrated twin boundary, as indicated by a white arrow in Fig. 9g. Fig. 9h suggests a higher accumulated density of geometrically necessary dislocations (GND) in the detwinned regions compressed to 10% strain. We argue that the higher local GND density serves as an effective obstacle for dislocation glide resulting in the observed hardening. This is in an agreement with non-mobile dislocations inherited from the operation of twinning, as was first proposed by Basinski et al. [40] for the case of a Cu-Al crystal. According to their observation, glissile dislocations before twinning convert to sessile configurations within twinned areas as a result of a twinning shear transformation. Consequently, these inherited dislocations will harden slip inside the twinned region [39]. In the case of Mg, this hardening mechanism, also called 'dislocation transmutation', has been experimentally observed by Wang and Agnew [41] and incorporated into a crystal plasticity model by El Kadiri and Oppedal [42]. Based on a dislocation reaction analysis on samples deformed up to a plateau region of stress-strain curves [41], $\langle a \rangle$ dislocations in the matrix may transmute into sessile $\langle c + a \rangle$ dislocations in the twin during the twinning operation. Accordingly, having such a KAM structure shown in Fig. 9h is

consistent with such debris associated with transmuted dislocations left behind in the wake of the detwinned boundary. This is one of the newest micromechanical supports of the 'dislocation transmutation' hardening mechanism in Mg.

A more in-depth inspection of KAM maps reveals the formation of a subgrain structure in both samples. These regions are indicated by dashed lines in Figs. 9c, 9d and 9h. The subgrain size is reflected by the expression of $w = bG/\sigma$ [43], where w, b, G and σ are the subgrain size, the magnitude of the Burgers vector, the shear modulus and the applied stress, respectively. Assuming the same Burgers vector and shear modulus for the two samples, the ratio of the subgrain size in the parent microcolumns over the detwinned microcolumns is inversely equal to the ratio of their stress levels. This ratio at 10% strain is roughly 1.40, taking the value of σ for the parent and detwinned microcolumns as 363 and 508 MPa, respectively. The calculated subgrain size ratio matches well the measurements from the KAM maps, where the subgrain size for the parent and detwinned microcolumns were measured to be ~806±174 nm and 560±157 nm, respectively. This stands for a roughly 1.44 times larger subgrain size for the parent microcolumns compared to the detwinned microcolumns. The smaller subgrain size in the detwinned microcolumn makes it more difficult for dislocations to squeeze through subgrains. This factor would also contribute to a more pronounced hardening effect for the detwinned microcolumns.

Furthermore, the observed local misorientations in the microcolumns will lead to local changes in the Schmid factor of the active slip system. This would directly contribute to a change of the stress required for plastic flow. The distribution of the highest Schmid factor for non-basal $\langle c + a \rangle$ slip systems was calculated for the cross-sections of the samples compressed to 5% strain. We calculated the Schmid factor distribution by knowing the Euler angles, the applied load direction, the slip direction and the slip plane normal for each measurement point in the samples cross-sections. The cumulative frequency distribution showed that the

bicrystalline microcolumn at the exhaustion of detwinning is less favored for subsequent $\langle c + a \rangle$ slip. By considering a Schmid factor of higher than 0.44 as a high potency to activate a slip system, 82% of the measurement points in the single crystal microcolumn, have these Schmid factor values. In the detwinned microcolumn, however, only 50% of the measurement points have this Schmid factor range. This means that the bicrystalline microcolumns require a higher resolved stress to initiate the plasticity through pyramidal slip after detwinning exhausts.

4. Summary

We performed compression experiments on single and bicrystalline Mg microcolumns to study the hardening mechanisms associated with detwinning of a single twin boundary. Our microcompression results showed that detwinning appears as a stress plateau in the stress-strain response of the bicrystalline microcolumns. Further straining of the detwinned microcolumns was associated with a hardening showing similar trends as found in the parent single crystal microcolumns. However, a significantly higher yield stress and a higher strain hardening rate was found in the detwinned microcolumns. Possible detwinning-mediated hardening mechanisms were discussed in terms of the microstructural observations made of the deformed volumes. We argued that simultaneous increase in yield strength and hardening rate of the detwinned microcolumns originates from the formation of dislocation debris formed in the wake of the detwinning front. While subgrain structures are formed in both samples, the cell size is smaller in the detwinned microcolumns. That, along with a relatively lower Schmid factor for subsequent pyramidal slip also led to the increased yield stress in the detwinned samples relative to the parent samples. Such a view of a detwinning mediated hardening is consistent with theoretical considerations found in the literature. Our experimental results suggests that any continuum-based modelling approaches to understanding the deformation of

Mg must include the concurrent mechanisms of twin migration and dislocation storage; simply reorienting the crystal upon twinning neglects critical aspects of the hardening response.

Figures:

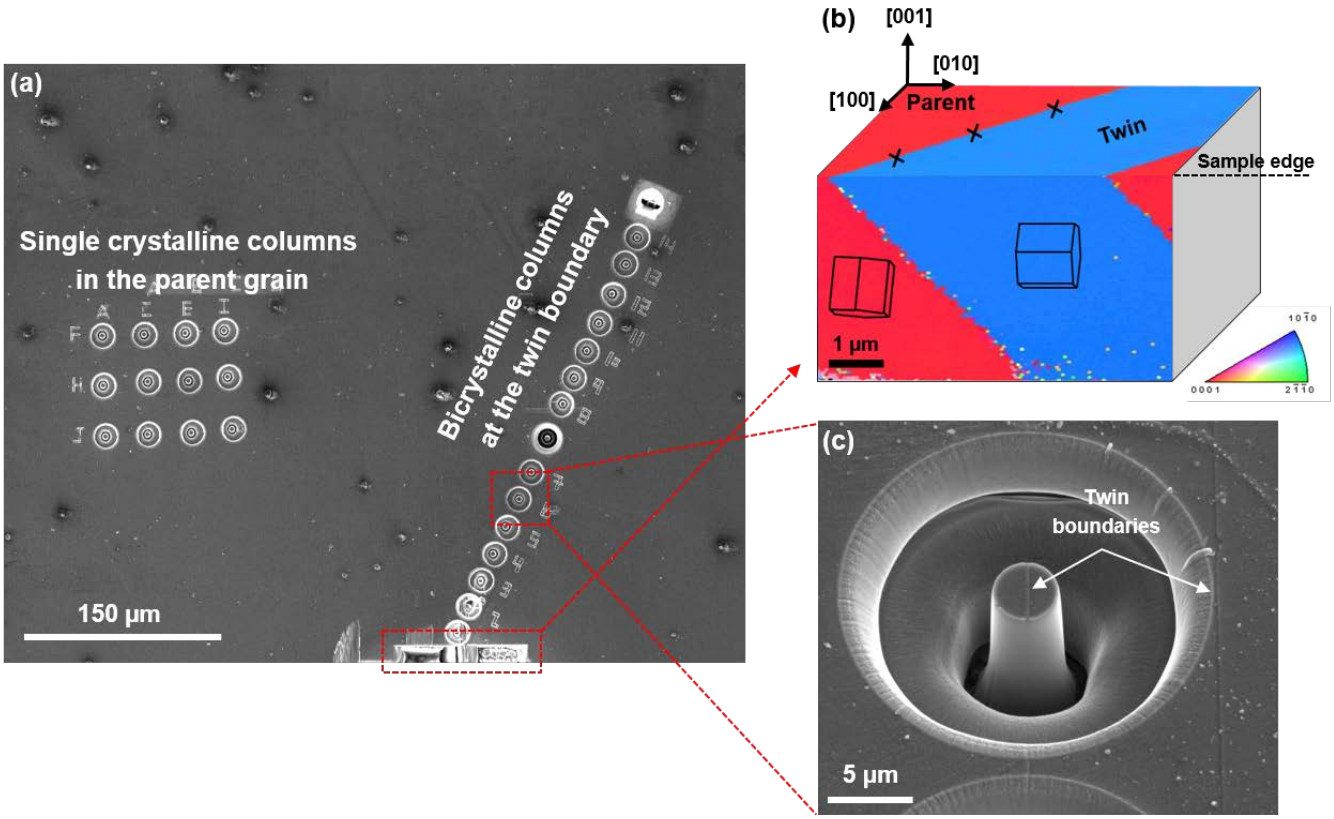

Figure 1. Fabricated microcolumns for micromechanical investigation. (a) Array of the samples in the selected parent grain and at the twin boundary, (b) [001] and [100] IPF maps showing the crystallographic arrangement of the parent grain and the twin and the location at which the columns were fabricated, and (c) a bicrystalline microcolumn machined such that the twin boundary is included in the column.

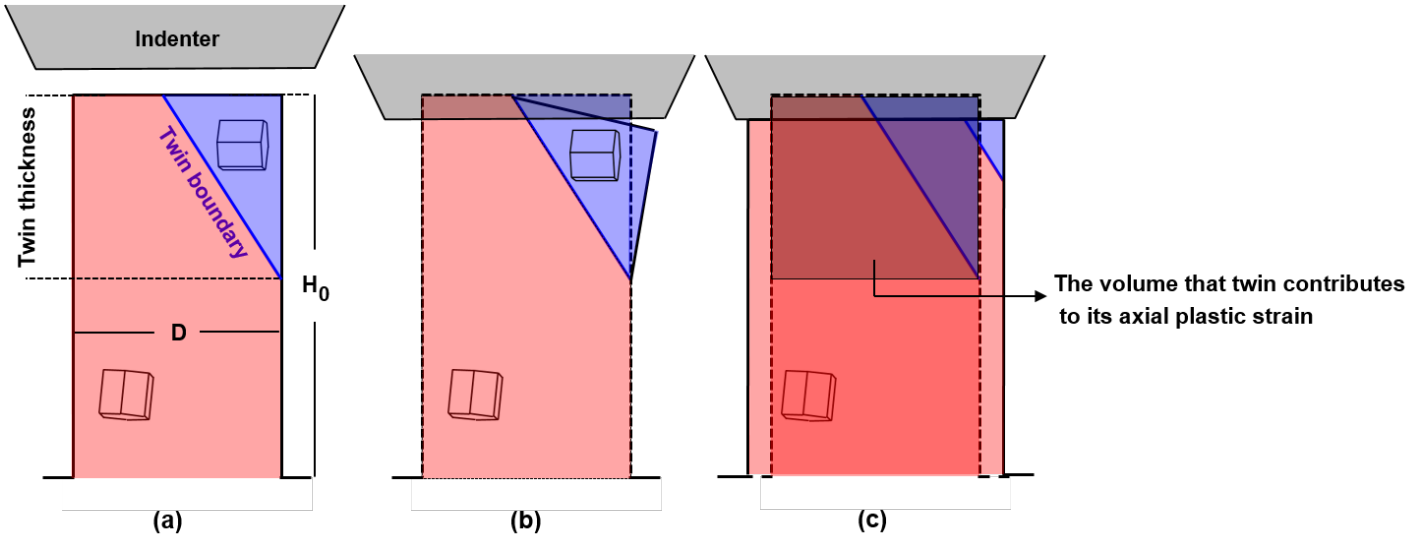

Figure 2. Schematic illustration of the compression of a bicrystalline microcolumn. (a) A cross-section of the column prior to compression, (b) constrained compatibility at the twin boundary and (c) a compressed column that has underwent detwinning. The dashed lines in (b) and (c) show the initial state before compression.

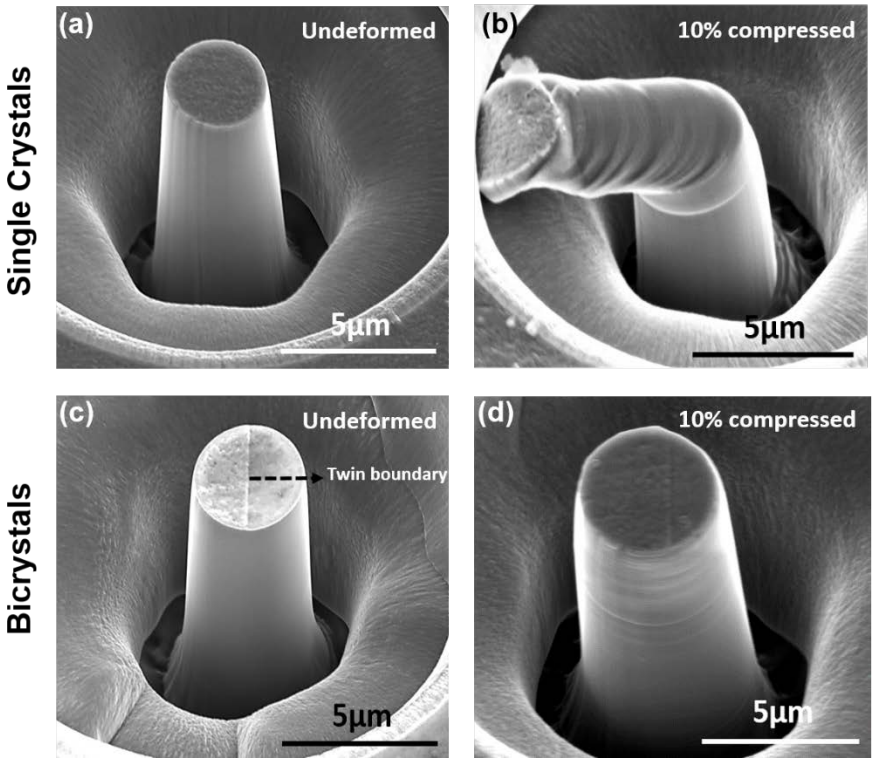

Figure 3. Post-mortem secondary electron images of the initial and compressed microcolumns. (a, b) Single crystals: (a) a column prior to microcompression and (b) a 10% compressed column. (c, d) Bicrystals: (c) an undeformed column containing the twin boundary and (d) a column after 10% compression.

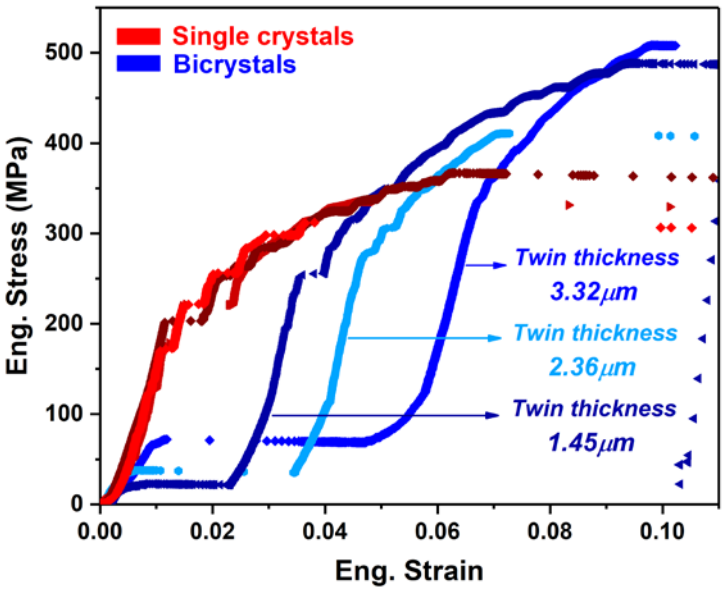

Figure 4. Engineering stress-strain curves for single (red) and bicrystalline (blue) microcolumns compressed to 10% engineering strain showing the different deformation behavior of the bicrystaline columns compared to the single crystals. The thickness of the twin included in bicrystals is also presented for each curve.

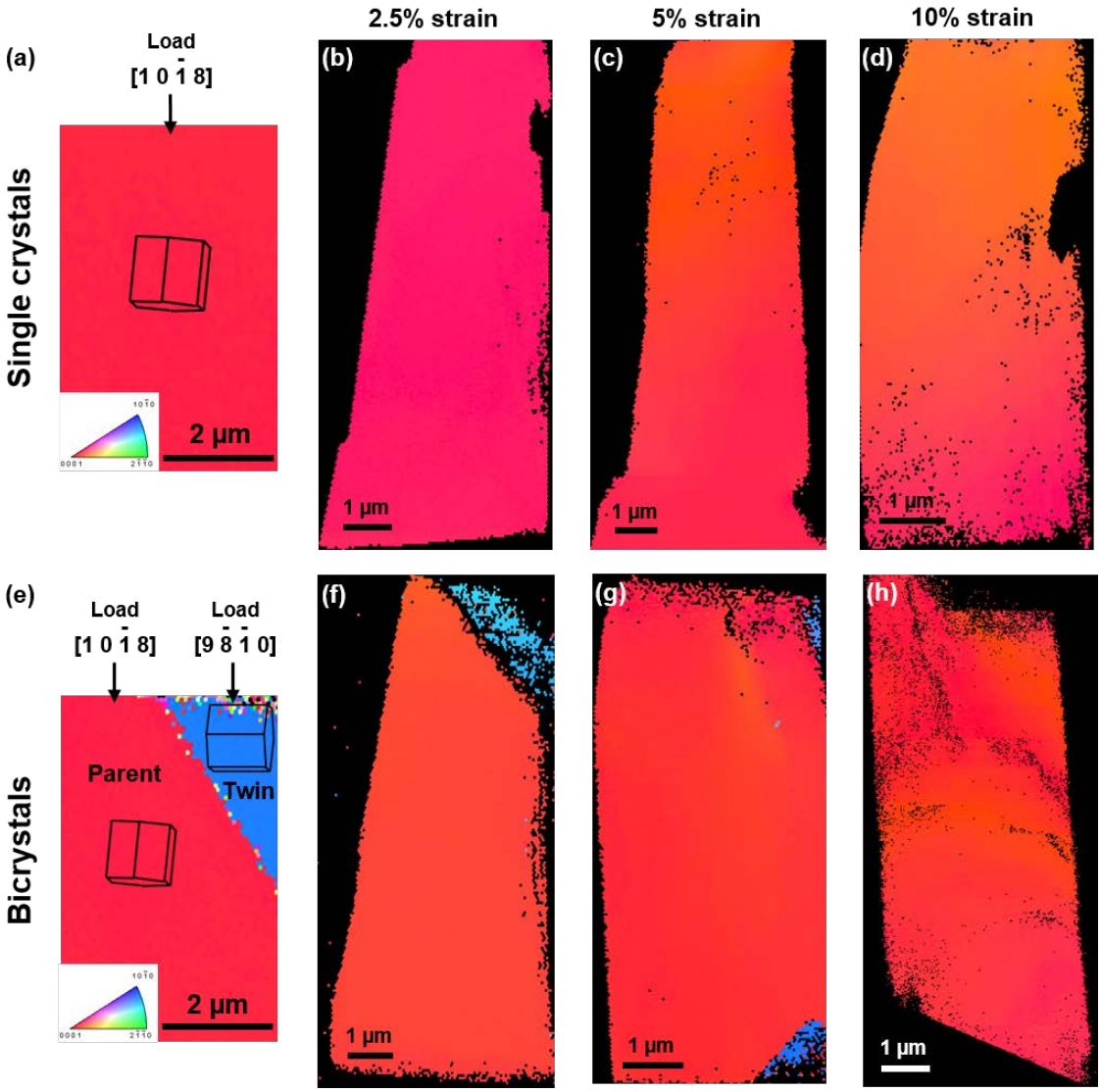

Figure 5. Microstructural observation of compressed microcolumns to varying strains shown by [100] IPF maps of samples cross-sections. (a-d) Single crystals: (a) undeformed 'parent' grain, columns after compression to (b) 2.5%, (c) 5% and (d) 10% strain. (e-h) Bicrystals: (e) undeformed parent-twin region, columns after compression to (f) 2.5%, (g) 5% and (h) 10% strain. Detwinning after compression of bicrystals is observed. The color-codes in (a) and (e) are valid for all pictures in their corresponding row.

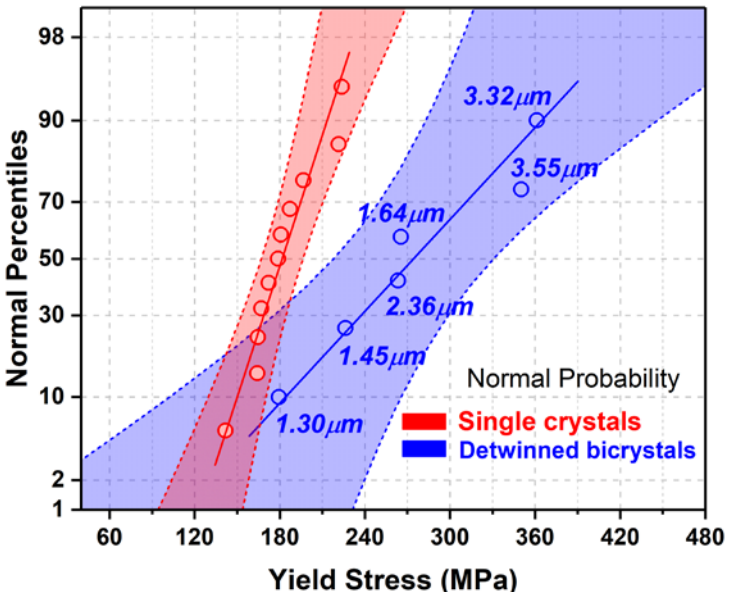

Figure 6. Normal probability plot of yield stress data obtained from the stress-strain curves of microcolumns compressed to 10% strain. The data for 11 single and 6 bicrystalline (after the plateau) columns are presented here. The figure shows seemingly higher yield stresses for the detwinned columns. Besides the best fit (solid lines), ±95% confidence intervals are given in colored regions with dashed line boundaries. The thickness of the twin boundary included in bicrystalline columns is also presented for the blue data points.

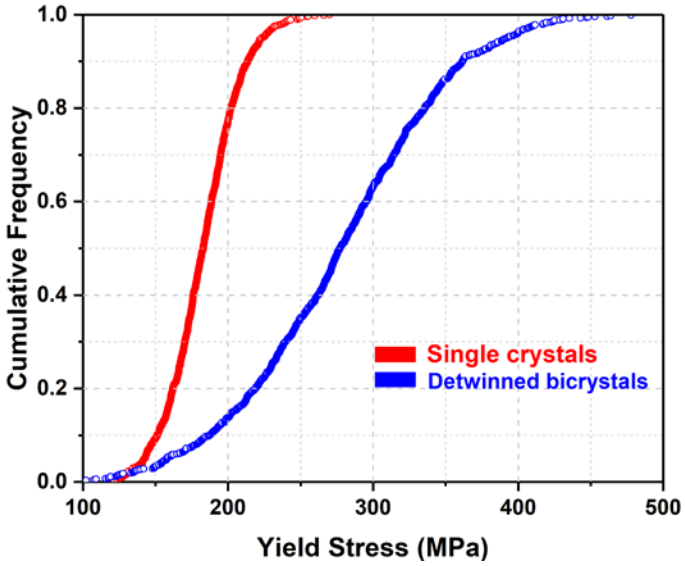

Figure 7. Cumulative frequency of 1000 randomly normal distributed yield stress dataset for single and bicrystalline microcolumns showing higher yield stress values for the samples that have underwent detwinning.

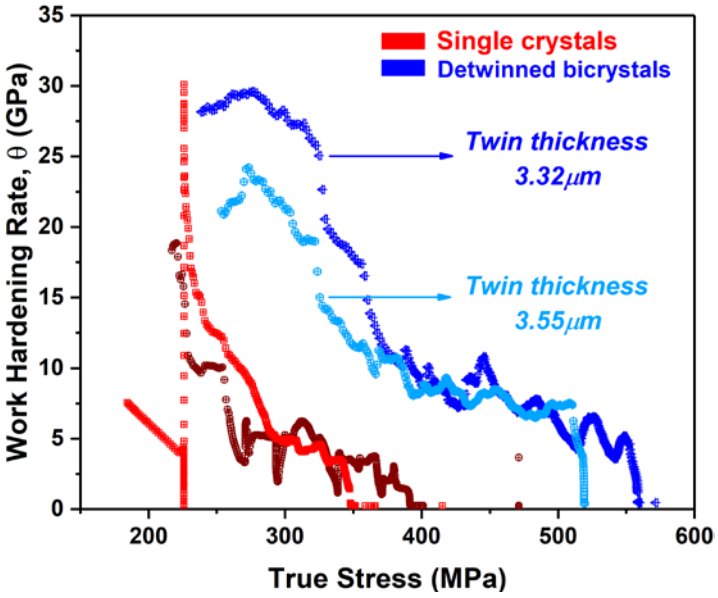

Figure 8. Work hardening rate as a function of true stress for microcolumns compressed to 10% strain. The curves for bicrystals have been plotted using the stress-strain data after the stress plateaus. Bicrystals show a distinguishable higher hardening rate after detwinning.

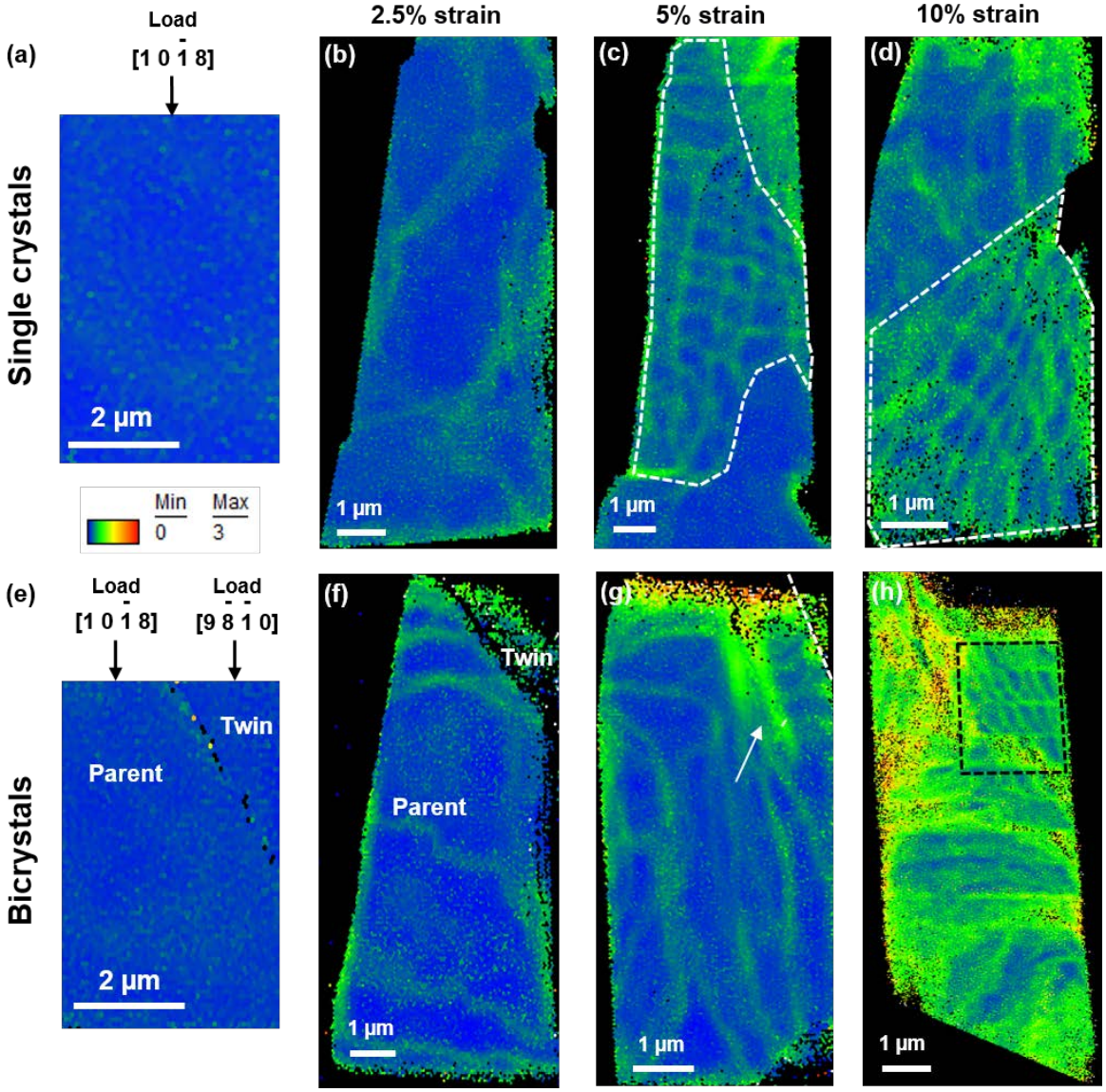

Figure 9. Maps of the kernel average misorientation for the compressed microcolumns to varying strains constructed from [100] IPF maps of the samples cross-sections. (a-d) Single crystals: (a) undeformed 'parent' grain, columns after compression to (b) 2.5%, (c) 5% and (d) 10% strain. (e-h) Bicrystals: (e) undeformed parent-twin region, columns after compression to (f) 2.5%, (g) 5%, the arrow and the withe dashed line show the initial and current location of the twin boundary, respectively and (h) 10% strain. Deformation of the detwinned column is associated with an inhomogeneous distribution of higher local misorientations compared to the single crystalline columns. Dashed lines indicate regions where a clear subgrain structure is formed.

Tables:

Table 1
Calculation of the contribution of detwinning in accommodating the axial strain.

Twin thickness (μm)	Detwinning strain % (Eq. 1)	Plateau strain %
1.30	0.7	2.9
1.45	0.7	2.3
1.64	0.8	3.1
2.36	1.2	3.4
3.32	1.7	4.8
3.55	1.8	5.5

References

1. Kocks, U. and D. Westlake, *The importance of twinning for the ductility of CPH polycrystals.* AIME MET SOC TRANS, 1967. **239**(7): p. 1107-1109.
2. Yoo, M. and J. Lee, *Deformation twinning in hcp metals and alloys.* Philosophical Magazine A, 1991. **63**(5): p. 987-1000.
3. Taylor, G.I., *Plastic strain in metals.* J. Inst. Metals, 1938. **62**: p. 307-324.
4. Christian, J.W. and S. Mahajan, *Deformation twinning.* Progress in materials science, 1995. **39**(1-2): p. 1-157.
5. Agnew, S.R. and Ö. Duygulu, *Plastic anisotropy and the role of non-basal slip in magnesium alloy AZ31B.* International Journal of plasticity, 2005. **21**(6): p. 1161-1193.
6. Barnett, M., *Twinning and the ductility of magnesium alloys: Part I:"Tension" twins.* Materials Science and Engineering: A, 2007. **464**(1-2): p. 1-7.
7. Hong, S.-G., S.H. Park, and C.S. Lee, *Role of {10–12} twinning characteristics in the deformation behavior of a polycrystalline magnesium alloy.* Acta Materialia, 2010. **58**(18): p. 5873-5885.
8. Lou, X., et al., *Hardening evolution of AZ31B Mg sheet.* International Journal of Plasticity, 2007. **23**(1): p. 44-86.
9. Cui, Y., et al., *Regulating twin boundary mobility by annealing in magnesium and its alloys.* International Journal of Plasticity, 2017. **99**: p. 1-18.
10. Cáceres, C., T. Sumitomo, and M. Veidt, *Pseudoelastic behaviour of cast magnesium AZ91 alloy under cyclic loading–unloading.* Acta Materialia, 2003. **51**(20): p. 6211-6218.
11. Lee, S. and M. Gharghouri, *Pseudoelastic behavior of magnesium alloy during twinning-dominated cyclic deformation.* Materials Science and Engineering: A, 2013. **572**: p. 98-102.
12. Muránsky, O., et al., *In situ neutron diffraction investigation of deformation twinning and pseudoelastic-like behaviour of extruded AZ31 magnesium alloy.* International Journal of Plasticity, 2009. **25**(6): p. 1107-1127.
13. Nie, J., et al., *Periodic segregation of solute atoms in fully coherent twin boundaries.* Science, 2013. **340**(6135): p. 957-960.
14. Cui, Y., et al., *Impact of solute elements on detwinning in magnesium and its alloys.* International Journal of Plasticity, 2017. **91**: p. 134-159.

15. Xin, Y., et al., *The different effects of solute segregation at twin boundaries on mechanical behaviors of twinning and detwinning.* Materials Science and Engineering: A, 2015. **644**: p. 365-373.
16. Xin, Y., et al., *Annealing hardening in detwinning deformation of Mg–3Al–1Zn alloy.* Materials Science and Engineering: A, 2014. **594**: p. 287-291.
17. Wang, Y. and J. Huang, *The role of twinning and untwinning in yielding behavior in hot-extruded Mg–Al–Zn alloy.* Acta materialia, 2007. **55**(3): p. 897-905.
18. Sarker, D. and D. Chen, *Detwinning and strain hardening of an extruded magnesium alloy during compression.* Scripta materialia, 2012. **67**(2): p. 165-168.
19. Cáceres, C. and A. Blake, *On the strain hardening behaviour of magnesium at room temperature.* Materials Science and Engineering: A, 2007. **462**(1-2): p. 193-196.
20. Cáceres, C., P. Lukáč, and A. Blake, *Strain hardening due to {10 1 2} twinning in pure magnesium.* Philosophical Magazine, 2008. **88**(7): p. 991-1003.
21. Nave, M.D. and M.R. Barnett, *Microstructures and textures of pure magnesium deformed in plane-strain compression.* Scripta Materialia, 2004. **51**(9): p. 881-885.
22. Kim, G.S., *Small volume investigation of slip and twinning in magnesium single crystals*. 2011, Grenoble.
23. Imrich, P.J., C. Kirchlechner, and G. Dehm, *Influence of inclined twin boundaries on the deformation behavior of Cu micropillars.* Materials Science and Engineering: A, 2015. **642**: p. 65-70.
24. Dehm, G., et al., *Overview on micro-and nanomechanical testing: New insights in interface plasticity and fracture at small length scales.* Acta Materialia, 2018. **142**: p. 248-282.
25. Mallmann, C., et al., *Influence of Y2O3 nanoparticles on the twinning of single crystalline magnesium.* Scripta Materialia, 2017. **138**: p. 79-82.
26. Hong, S.-G., S.H. Park, and C.S. Lee, *Strain path dependence of {1 0− 1 2} twinning activity in a polycrystalline magnesium alloy.* Scripta Materialia, 2011. **64**(2): p. 145-148.
27. Yoo, M., *Slip, twinning, and fracture in hexagonal close-packed metals.* Metallurgical Transactions A, 1981. **12**(3): p. 409-418.
28. Kheradmand, N., et al., *Microscopic incompatibility controlling plastic deformation of bicrystals.* Acta Materialia, 2016. **106**: p. 219-228.
29. Lilleodden, E., *Microcompression study of Mg (0 0 0 1) single crystal.* Scripta Materialia, 2010. **62**(8): p. 532-535.
30. Byer, C.M. and K. Ramesh, *Effects of the initial dislocation density on size effects in single-crystal magnesium.* Acta Materialia, 2013. **61**(10): p. 3808-3818.
31. Liu, Y., et al., *Experimentally quantifying critical stresses associated with basal slip and twinning in magnesium using micropillars.* Acta Materialia, 2017. **135**: p. 411-421.
32. Prasad, K.E., K. Rajesh, and U. Ramamurty, *Micropillar and macropillar compression responses of magnesium single crystals oriented for single slip or extension twinning.* Acta Materialia, 2014. **65**: p. 316-325.
33. Volkert, C.A. and E.T. Lilleodden, *Size effects in the deformation of sub-micron Au columns.* Philosophical Magazine, 2006. **86**(33-35): p. 5567-5579.
34. Kupka, D., N. Huber, and E. Lilleodden, *A combined experimental-numerical approach for elasto-plastic fracture of individual grain boundaries.* Journal of the Mechanics and Physics of Solids, 2014. **64**: p. 455-467.
35. Malyar, N., et al., *Dislocation slip transmission through a coherent Σ3 {111} copper twin boundary: Strain rate sensitivity, activation volume and strength distribution function.* Acta Materialia, 2018. **161**: p. 412-419.
36. Knezevic, M., et al., *Deformation twinning in AZ31: influence on strain hardening and texture evolution.* Acta Materialia, 2010. **58**(19): p. 6230-6242.
37. Wonsiewicz, B.C., *Plasticity of magnesium crystals*. 1966, Massachusetts Institute of Technology.

38. Clausen, B., et al., *Reorientation and stress relaxation due to twinning: modeling and experimental characterization for Mg.* Acta Materialia, 2008. **56**(11): p. 2456-2468.
39. Proust, G., et al., *Modeling the effect of twinning and detwinning during strain-path changes of magnesium alloy AZ31.* International Journal of Plasticity, 2009. **25**(5): p. 861-880.
40. Basinski, Z., et al., *The transformation of slip dislocations during twinning of copper-aluminum alloy crystals.* Revue de mEtallurgie, 1997. **94**(9): p. 1037-1044.
41. Wang, F. and S.R. Agnew, *Dislocation transmutation by tension twinning in magnesium alloy AZ31.* International Journal of Plasticity, 2016. **81**: p. 63-86.
42. El Kadiri, H. and A. Oppedal, *A crystal plasticity theory for latent hardening by glide twinning through dislocation transmutation and twin accommodation effects.* Journal of the Mechanics and Physics of Solids, 2010. **58**(4): p. 613-624.
43. Sedláček, R., et al., *Subgrain formation during deformation: physical origin and consequences.* Metallurgical and Materials Transactions A, 2002. **33**(2): p. 319-327.